Aggregation

Deutsche Ausgabe: DOI: 10.1002/ange.201500129
Internationale Ausgabe: DOI: 10.1002/anie.201500129

o-Carborane-Based Anthracene: A Variety of Emission Behaviors**

Hirofumi Naito, Yasuhiro Morisaki, and Yoshiki Chujo**

Abstract: *An o-carborane-based anthracene was synthesized, and single crystals, with incorporated solvent molecules, were obtained from the $CHCl_3$, CH_2Cl_2, and C_6H_6 solutions. The anthracene ring in the crystal is highly distorted by the formation of a π-stacked dimer between the anthracene units. The crystals exhibited a variety of emission behaviors such as aggregation-induced emission (AIE), crystallization-induced emission (CIE), aggregation-caused quenching (ACQ), and multichromism.*

O-Carborane ($C_2B_{10}H_{12}$) is a polyhedral boron cluster compound which includes two adjacent carbon atoms in the cluster cage.[1] The applications of carboranes for use in boron neutron capture therapy and for heat-resistant materials have been extensively studied because of their high boron content and thermal and chemical stability.[1,2] Recently, the construction of π-conjugated systems including the *o*-carborane moiety for applications as light-emitting materials has received significant attention.[3,4] Previously, we reported the syntheses of π-conjugated compounds in which π-electron systems were attached at the C1 and C2 positions of *o*-carborane, and found that they exhibited aggregation-induced emission (AIE).[4] The AIE properties[5] of *o*-carborane-based conjugated systems are caused by intramolecular charge transfer from the π-conjugated groups to *o*-carborane,[3e] and emission results from the restricted molecular motion of the *o*-carborane cage in the aggregated state or in frozen media at 77 K. To date, the synthesis and unique emission behaviors of AIE-active *o*-carborane derivatives have been reported. In addition to AIE properties, Tang and co-workers also reported a crystallization-induced emission (CIE) property.[6] Emission from the π-conjugated system in these molecules can be induced efficiently in the crystal state. Generally, luminescence properties of emissive molecules depend on the solid state and are influenced by various factors such as crystallinity, amorphous character, and solvent-molecule incorporation. Appropriate control of the compounds in the solid state leads to external stimuli-responsive luminescent materials.[7]

From this viewpoint, we attempted to synthesize an *o*-carborane-based stimuli-responsive compound. We selected anthracene as the π-electron system because of its prominent luminescent properties and facile functionalization.[8–10] Furthermore, the luminescent colors of anthracene derivatives in the solid state can be modified by varying their assemblies. Herein, we report the synthesis of *o*-carborane-based anthracene,[10] in which *o*-carboranes are substituted at the 9- and 10-positions of anthracene. The structures and their unprecedented emission behaviors such as AIE, CIE, aggregation-caused quenching (ACQ), thermochromism, vapochromism, and mechanochromism are discussed in detail.

As shown in Scheme 1, the compound **3** was synthesized from decaborane ($B_{10}H_{14}$; **1**), CH_3CN,[11a] and 9,10-di(phenylethynyl)anthracene (**2**) using $AgNO_3$ as a Lewis acid.[11b] Recrystallization of **3** from $CHCl_3$ afforded the corresponding solvent cocrystal **3**·$CHCl_3$ in 23% yield. The compound **3**·$CHCl_3$ was stable to H_2O, air, and heat in both solution and solid states. In addition, thermogravimetric analysis (TGA) of **3**·$CHCl_3$ showed that decomposition started at approximately 340 °C under N_2, as shown in Figure S19 (see the Supporting Information). Furthermore, photoinduced dimerization of the anthracene units in **3**·$CHCl_3$ did not occur under UV irradiation in air. Thus, the anthracene ring is stabilized thermodynamically and kinetically by the electron-withdrawing character[12] of *o*-carborane and steric hindrance of the phenyl-substituted *o*-carborane, respectively.

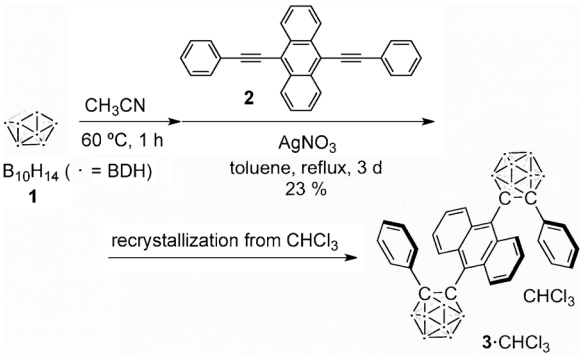

Scheme 1. Synthesis of *o*-carborane-based anthracene.

Figure 1 shows the UV-vis absorption spectra of a dilute THF solution (1.0×10^{-5} M) of **3** and the aggregates in a THF/H_2O solution (v/v = 1/99, 1.0×10^{-5} M). Both spectra exhibited the typical π–π* bands of the anthracene moiety at approximately $\lambda = 280$ and 450 nm, and that of the phenyl group at around $\lambda = 280$ nm. Figure 1 also shows the photoluminescence (PL) spectra of the THF solution, aggregates, and the crystal of **3**·$CHCl_3$. The spectrum of the dilute THF solution exhibited a weak peak at $\lambda = 650$ nm which is derived from

[*] H. Naito, Prof. Y. Morisaki, Prof. Y. Chujo
Department of Polymer Chemistry
Graduate School of Engineering, Kyoto University
Katsura, Nishikyo-ku, Kyoto 615-8510 (Japan)
E-mail: ymo@chujo.synchem.kyoto-u.ac.jp
chujo@chujo.synchem.kyoto-u.ac.jp

[**] This work was partially supported by Grant-in-Aid for Scientific Research on Innovative Areas "Element-Blocks" (No. 24102013) from the MEXT.

Supporting information for this article is available on the WWW under http://dx.doi.org/10.1002/anie.201500129.

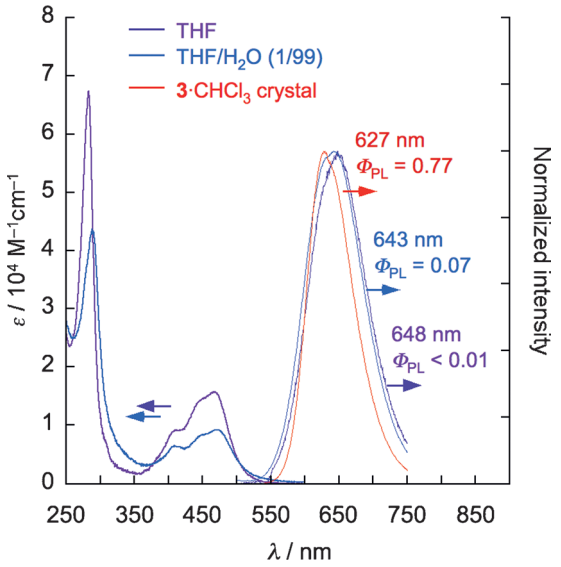

Figure 1. Absorption spectra of **3** in THF (1.0×10^{-5} M) and the aggregates (THF/H_2O v/v = 1:99 solution, 1.0×10^{-5} M). Normalized PL spectra of **3** in THF (1.0×10^{-5} M), the aggregates (THF/H_2O = 1:99 solution, 1.0×10^{-5} M), and the **3**·$CHCl_3$ crystal (excited at $\lambda = 470$ nm).

charge-transfer[3e] (CT) emission of the di(*o*-carboranyl)-anthracene moiety.[13] The absolute PL quantum efficiency (Φ_{PL}) of the dilute THF solution was less than 0.01 ($\tau = 9.2$ ns, $\chi^2 = 1.18$). From the aggregates, only CT emission was observed at $\lambda = 643$ nm (Figure 1) with a slightly higher Φ_{PL} value of 0.07 ($\tau = 8.8$ ns, $\chi^2 = 1.13$). The compound **3** exhibited a broad emission peak in the same region in frozen media (2-methyl-THF at 77 K, 1.0×10^{-5} M; see Figure S5 in the Supporting Information), thus indicating that the broad peak results from the AIE which arises because of the suppression of C–C bond vibration in the *o*-carborane and that emission from the aggregates in THF/H_2O (v/v 1:99) was bathochromically shifted because of the increase in the polarity by H_2O. The most efficient emission (CIE) was observed from the crystal of **3**, with a calculated Φ_{PL} value of 0.77.

To better understand the CIE properties of **3**, its single crystals were obtained from CH_2Cl_2 and C_6H_6 solutions, in addition to a $CHCl_3$ solution, for X-ray crystallography. As shown in Figure 2 A, the anthracene rings of two molecules of **3** form a π-stacked dimer and each solvent molecule is incorporated into each crystal lattice (see Figures S7–S9 in the Supporting Information). The overlapping area of two π-stacked anthracenes were estimated as 11, 12, and 19% for **3**·CH_2Cl_2, **3**·C_6H_6, and **3**·$CHCl_3$, respectively (Figure 2 A). The PL spectra of the crystals were then correlated to the difference in the overlapping percentages and distances between centers of anthracenes. The emission peak was observed at a longer wavelength for crystal structures which have a greater overlap and shorter distance between the two anthracenes in the stacked dimer (Figure 2 B).[14,15] In contrast to emission from solution and aggregates, CIE consisted of two decay components (see Table S5 in the Supporting Information), that is, anthracene stacking influenced the CT emission, depending on the stacking distance and overlapping

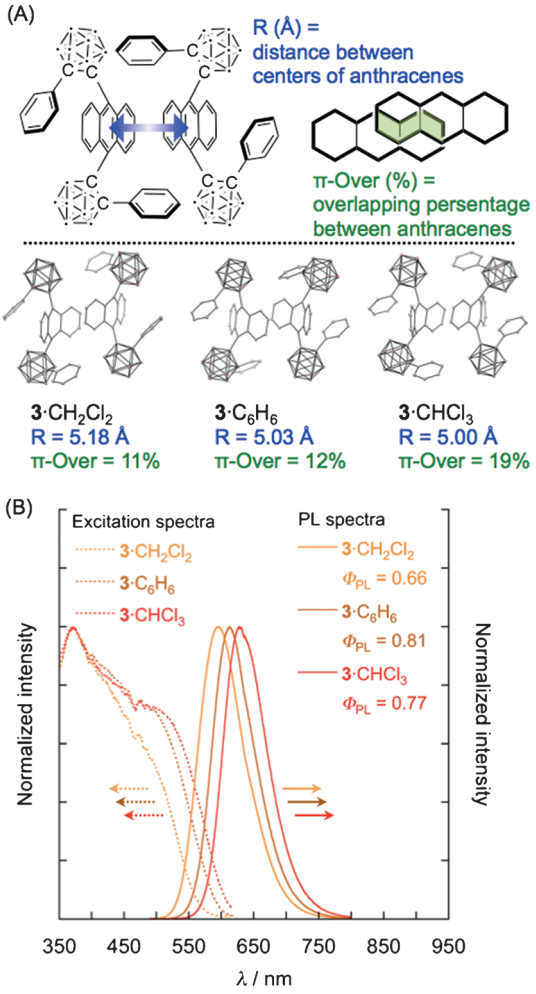

Figure 2. A) Structure of π-stacked dimer and ORTEP drawings of **3**·CH_2Cl_2, **3**·C_6H_6, and **3**·$CHCl_3$. B) Excitation and PL spectra of **3**·CH_2Cl_2, **3**·C_6H_6, and **3**·$CHCl_3$ crystals. Excitation spectra were monitored at 594 nm for **3**·CH_2Cl_2, 613 nm for **3**·C_6H_6, and 627 nm for **3**·$CHCl_3$.

percentage rather than on the solvatochromic effect by the incorporated solvent molecules. Bathochromic shifts in the excitation spectra were also observed, and correspond to the overlapping percentage and distance between anthracenes (Figure 2 B).

Interestingly, distortion of the anthracene ring was observed in the **3**·solvent crystals. The ring strain was evaluated with ring deformation angles α and β for the central ring, as shown in Figure S10 in the Supporting Information. The α and β values for the central rings of anthracene in **3**·$CHCl_3$ were 21.5° and 6.4°, respectively. For comparison, the deformation angles α and β of [6]-(9,10)anthracenophane are 24.7° and 18.5°,[16a] respectively, and those of [1,1](9,10)anthracenophane are 16.3° and 5.8°,[16b] respectively.[17] Therefore, the anthracene ring in the **3**·$CHCl_3$ crystal is significantly distorted despite the fact that **3** is not a strained cyclophane compound. These large deformation angles are a result of π–π interactions between the anthracene rings and steric hindrance of the phenyl-substituted *o*-carboranes in the π-stacked dimer. The aromaticity of the anthracene rings in the **3**·solvent crystals was studied by

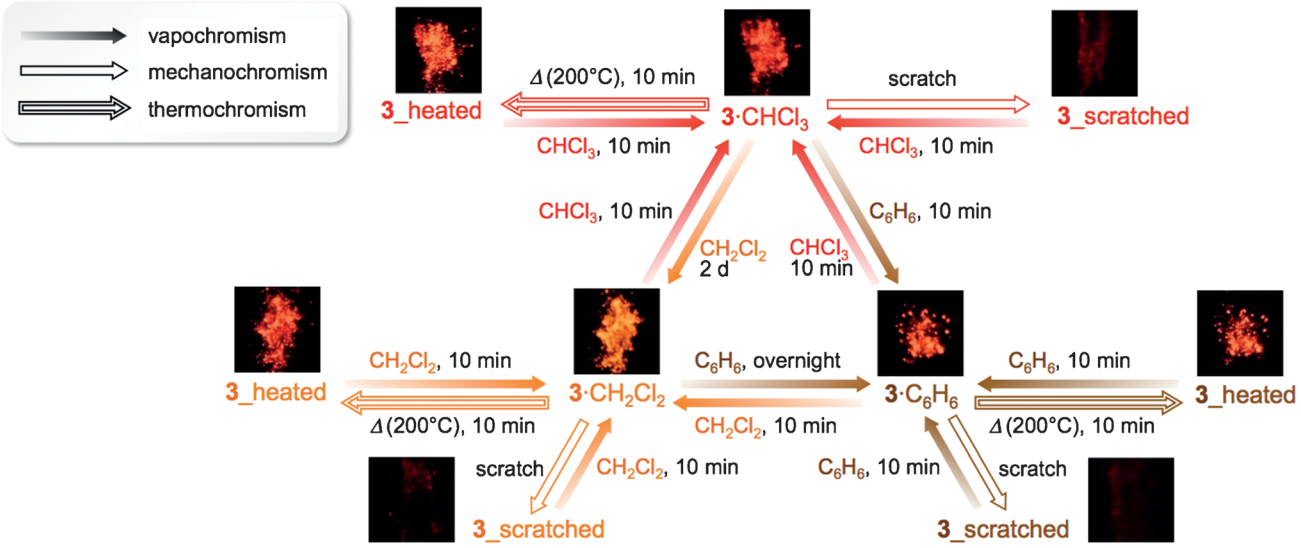

Figure 3. Thermochromism, vapochromism, and mechanochromism of the **3**·solvent crystals.

nucleus-independent chemical shifts (NICS; see Table S4) and the results suggest that their aromaticity is maintained.

As shown in Figure 3, crystals of **3**·solvent exhibited reversible thermochromism, vapochromism, and mechanochromism, and PL spectra and X-ray diffraction (XRD) patterns were measured after each step (see Figures S23–S40 in the Supporting Information). Heating the crystals at 200 °C for 10 minutes under air resulted in the loss of solvent molecules from the crystals, and thus changes in their emission behavior. The loss of solvent molecules was confirmed by TGA, differential scanning calorimetry (DSC; see Figures S17–22 in the Supporting Information), and X-ray fluorescence (XRF)[18] analysis. For example, 86 % of the CH_2Cl_2 molecules in **3**·CH_2Cl_2 were removed from the crystal by heating (see Figure S41 in the Supporting Information). Almost identical PL spectra (see Figure S12 in the Supporting Information) and excitation spectra (Figure S15) were observed after heating, and good Φ_{PL} values were obtained (Table S5). When the heated solids were exposed to solvent vapor for 10 minutes in a Petri dish, the PL profile and XRD pattern of the crystal corresponding to each solvent was reversibly observed (see Figures S23, S24, S27, S28, S31, and S32).

Next, the response of the to a mechanical stimulus was monitored by PL. Scratching the crystals with a spatula or grinding with a mortar and a pestle dramatically decreases the Φ_{PL} value (see Figure S13 and Table S5). For example, the Φ_{PL} value of **3**·CH_2Cl_2 changed from 0.66 to 0.08. In addition, the PL and excitation spectra for the scratched solid were bathochromically shifted (see Figure S13 and S16, respectively). The XRD pattern of **3**·CH_2Cl_2 before scratching exhibited sharp peaks, whereas the scratched solid exhibited no clear signals (see Figure S26). Similar to the heated crystals, the XRF results show that approximately 97 % of CH_2Cl_2 was removed from **3**·CH_2Cl_2 by scratching (see Figure S41). These results suggest that the crystals of **3**·CH_2Cl_2 become amorphous after mechanical stress-induced loss of CH_2Cl_2 molecules, thus leading to the ACQ. However, annealing the scratched solids with CH_2Cl_2 vapor resulted in the PL spectrum and XRD pattern (see Figure S25 and 26, respectively) identical to those of the original **3**·CH_2Cl_2 crystals. This scratching and solvent annealing process could be repeatedly carried out at least ten times (see Figure S43), which demonstrates the robust reversible mechanochromism of the **3**·CH_2Cl_2 crystals. It seems that access of solvent is relatively easy because there is sufficient space, and there are no interactions such as π–π and CH—π interactions between **3** and solvent molecules in the crystals, according to the X-ray crystallography.

Intrigued by the repeatability of the annealing process, we next tested substitution of the solvent in the crystals. Exposure of the crystals to a different solvent vapor in a Petri dish at room temperature afforded the desired substitution. Although the substitution time depended on the solvent and crystal, the PL and XRD changes were observed in all cases (see Figure S35–40).

In conclusion, *o*-carborane-substituted anthracene was successfully synthesized and characterized. Single crystals were obtained from CH_2Cl_2, $CHCl_3$, and C_6H_6 solutions, and each solvent molecule was incorporated into the crystals. In the crystal, the anthracene ring was highly distorted because of the formation of a π-stacked dimer between anthracene units. A wide variety of emission behaviors were observed for the crystals, including AIE, CIE, ACQ, thermochromism, vapochromism, and mechanochromism. Based on these results, bis(*o*-carborane)-substituted acenes are promising skeletons for solid stimuli-responsive emissive materials.

Experimental Section

Decaborane (**1**; 1.51 g, 12.3 mmol) was dissolved in CH_3CN (2.5 mL) at room temperature under Ar atmosphere.[1a] The mixture was stirred for 1 h at 60 °C, and then, 9,10-bis(phenylethynyl)anthracene (**2**; 1.40 g, 3.7 mmol), $AgNO_3$[1b] (54 mg, 0.32 mmol), and dry toluene (40 mL) were added. The mixture was refluxed for 3 days. After cooling to room temperature, solvent was evaporated, and the residue

was purified by column chromatography on silica gel (*n*-hexane/CH_2Cl_2 v/v = 3:2). After evaporation of solvent, recrystallization from $CHCl_3$ was carried out to afford **3**·$CHCl_3$ as a red single crystal (0.68 g, 1.10 mmol, 30% yield based on **1**). ^{1}H NMR (400 MHz, CD_2Cl_2): δ = 8.60 (4H, dd, J = 7.08 Hz, J = 3.16 Hz, Ar-*H*), 7.30–7.26 (10H, m, Ar-*H*), 7.06 (4H, t, J = 7.92 Hz, Ar-*H*), 3.2–1.6 ppm (20H, br, B-*H*). ^{13}C NMR (100 MHz, CD_2Cl_2): δ = 133.7, 132.4, 131.4, 129.9, 129.3, 126.4, 125.3, 125.1, 91.8, 88.5 ppm. ^{11}B NMR (128 MHz, CD_2Cl_2): δ = −1.2, −2.3, −4.5, −5.7, −10.4, −11.5 ppm. HRMS (APCI): Calcd. for $C_{30}H_{38}B_{20}$ $[M+H]^+$ m/z 619.4977, found m/z 619.4969. Single crystals of **3**·CH_2Cl_2 and **3**·C_6H_6 were obtained as follows. Crystal of **3**·$CHCl_3$ (2 mg) was dissolved in CH_2Cl_2 or C_6H_6 (0.5 mL). Slow evaporation of the solution at room temperature afforded the corresponding single crystal **3**·CH_2Cl_2 or **3**·C_6H_6.

Keywords: aggregation · carboranes · crystal growth · luminescence · solid-state structures

How to cite: *Angew. Chem. Int. Ed.* **2015**, *54*, 5084–5087
Angew. Chem. **2015**, *127*, 5173–5176

[1] a) "Icosahedral carboranes: 1,2-$C_2B_{10}H_{12}$": R. N. Grimes in *Carboranes*, 2nd ed., Academic Press, New York, **2011**, chap. 9, pp. 301–540; b) B. P. Dash, R. Satapathy, J. A. Maguireb, N. S. Hosmane in *Boron Science: New Technologies and Applications* (Ed.: N. S. Hosmane), CRC, Boca Raton, FL, **2011**, pp. 675–699.

[2] a) V. I. Bregadze, *Chem. Rev.* **1992**, *92*, 209–223; b) A. González-Campo, E. J. Juárez-Pérez, C. Viñas, B. Boury, R. Sillanpää, R. Kivekäs, R. Núñez, *Macromolecules* **2008**, *41*, 8458–8466; c) F. Issa, M. Kassiou, L. M. Rendina, *Chem. Rev.* **2011**, *111*, 5701–5722; d) A. Ferrer-Ugalde, E. J. Juárez-Pérez, F. Teixidor, C. Viñas, R. Núñez, *Chem. Eur. J.* **2013**, *19*, 17021–17030.

[3] a) J. J. Peterson, M. Werre, Y. C. Simon, E. B. Coughlin, K. R. Carter, *Macromolecules* **2009**, *42*, 8594–8598; b) F. Lerouge, A. Ferrer-Ugalde, C. Viñas, F. Teixidor, A. Abreu, E. Xochitiotzi, N. Farfán, R. Santillan, R. Sillanpää, R. Núñez, *Dalton Trans.* **2011**, *40*, 7541–7550; c) B. P. Dash, R. Satapathy, E. R. Gaillard, K. M. Norton, J. A. Maguire, N. Chug, N. S. Hosmane, *Inorg. Chem.* **2011**, *50*, 5485–5493; d) A. R. Davis, J. J. Peterson, K. R. Carter, *ACS Macro Lett.* **2012**, *1*, 469–472; e) K.-R. Wee, W.-S. Han, D. W. Cho, S. Kwon, C. Pac, S. O. Kang, *Angew. Chem. Int. Ed.* **2012**, *51*, 2677–2680; *Angew. Chem.* **2012**, *124*, 2731–2734; f) Y. Morisaki, M. Tominaga, Y. Chujo, *Chem. Eur. J.* **2012**, *18*, 11251–11257; g) K.-R. Wee, Y.-J. Cho, S. Jeong, S. Kwon, J.-D. Lee, I.-H. Suh, S. O. Kang, *J. Am. Chem. Soc.* **2012**, *134*, 17982–17990; h) H. J. Bae, H. Kim, K. M. Lee, T. Kim, Y. S. Lee, Y. Do, M. H. Lee, *Dalton Trans.* **2014**, *43*, 4978–4985.

[4] a) K. Kokado, Y. Chujo, *Macromolecules* **2009**, *42*, 1418–1420; b) K. Kokado, Y. Chujo, *J. Org. Chem.* **2011**, *76*, 316–319.

[5] a) *Aggregation-induced emission: Fundamentals* (Eds.: A. Qin, B. Z. Tang), Wiley, New York, **2013**; b) *Aggregation-induced emission: Applications* (Eds. A. Qin, B. Z. Tang), Wiley, New York, **2013**; c) J. Luo, Z. Xie, J. W. Y. Lam, L. Cheng, H. Chen, C. Qiu, H. S. Kwok, X. Zhan, Y. Liu, D. Zhu, B. Z. Tang, *Chem. Commun.* **2001**, 1740–1741.

[6] a) Y. Dong, J. W. Y. Lam, A. Qin, Z. Li, J. Sun, H. H.-Y. Sung, I. D. Williams, B. Z. Tang, *Chem. Commun.* **2007**, 40–42; b) Y. Dong, J. W. Y. Lam, A. Qin, J. Sun, J. Liu, Z. Li, J. Sun, H. H.-Y. Sung, I. D. Williams, H. S. Kwok, B. Z. Tang, *Chem. Commun.* **2007**, 3255–3257.

[7] a) Y. Sagara, T. Kato, *Nat. Chem.* **2009**, *1*, 605–610; b) D. A. Davis, A. Hamilton, J. Yang, L. D. Cremar, D. Van Gough, S. L. Potisek, M. T. Ong, P. V. Braun, T. J. Martinez, S. R. White, J. S. Moore, N. R. Sottos, *Nature* **2009**, *459*, 68–72; c) X. Zhang, Z. Chi, Y. Zhang, S. Liu, J. Xu, *J. Mater. Chem. C* **2013**, *1*, 3376–3390.

[8] a) X. Zhang, Z. Chi, B. Xu, L. Jiang, X. Zhou, Y. Zhang, S. Liu, J. Xu, *Chem. Commun.* **2012**, *48*, 10895–10897; b) M. R. Rao, C.-W. Liao, W.-L. Su, S.-S. Sun, *J. Mater. Chem. C* **2013**, *1*, 5491–5501; c) B. Chen, G. Yu, X. Li, Y. Ding, C. Wang, Z. Liu, Y. Xie, *J. Mater. Chem. C* **2013**, *1*, 7409–7417; d) Y. Dong, J. Zhang, X. Tan, L. Wang, J. Chen, B. Li, L. Ye, B. Xu, B. Zou, W. Tian, *J. Mater. Chem. C* **2013**, *1*, 7554–7559; e) X. Zhang, Z. Ma, Y. Yang, X. Zhang, Z. Chi, S. Liu, J. Xu, X. Jia, Y. Wei, *Tetrahedron* **2014**, *70*, 924–929.

[9] a) Y. Mizobe, N. Tohnai, M. Miyata, Y. Hasegawa, *Chem. Commun.* **2005**, 1839–1841; b) Y. Mizobe, T. Hinoue, A. Yamamoto, I. Hisaki, M. Miyata, Y. Hasegawa, N. Tohnai, *Chem. Eur. J.* **2009**, *15*, 8175–8184; c) Z. Zhang, Y. Zhang, D. Yao, H. Bi, I. Javed, Y. Fan, H. Zhang, Y. Wang, *Cryst. Growth Des.* **2009**, *9*, 5069–5076; d) T. Hinoue, Y. Doi, Y. Mizobe, I. Hisaki, M. Miyata, N. Tohnai, *Chem. Eur. J.* **2012**, *18*, 4634–4643.

[10] a) A. Sousa-Pedrares, C. Vinas, F. Teixidor, *Chem. Commun.* **2010**, *46*, 2998–3000; b) A. Ferrer-Ugalde, A. González-Campo, C. Viñas, J. Rodríguez-Romero, R. Santillan, N. Farfán, R. Sillanpää, A. Sousa-Pedrares, R. Núñez, F. Teixidor, *Chem. Eur. J.* **2014**, *20*, 9940–9951.

[11] a) R. Schaeffer, *J. Am. Chem. Soc.* **1957**, *79*, 1006–1007; b) A. Toppino, A. R. Genady, M. E. El-Zaria, J. Reeve, F. Mostofian, J. Kent, J. F. Valliant, *Inorg. Chem.* **2013**, *52*, 8743–8749.

[12] The reversible cyclic voltammogram of **3** is shown in Figure S6. The lowest unoccupied molecular orbital (LUMO) potential was calculated to be −4.16 eV, which is similar to the value for C_{60} (−4.2 eV). Electrochemical behaviors of *o*-carborane-based conjugated compounds (e.g., 2e reduction of a carborane unit) were reported by Weber, Fox, and co-workers. See: L. Weber, J. Kahlert, L. Böhling, A. Brockhinke, H.-G. Stammler, B. Neumann, R. A. Harder, P. J. Low, M. A. Fox, *Dalton Trans.* **2013**, *42*, 2266–2281.

[13] Highest occupied molecular orbital (HOMO) and lowest unoccupied molecular orbital (LUMO) of pristine and distorted compounds **3** are shown in Figure S44 (see the Supporting Information). Both LUMOs were delocalized on anthracene and carborane moieties through the overlap between the π*-orbital of anthracene and the antibonding orbital of the C1–C2 bond in the carborane cage, which caused CT. Solvatochromic effect of **3** was also investigated, and the result is shown in Figure S45 in the Supporting Information. The linear relationship was observed in the Lippert–Mataga plot, thus supporting the CT emission. For the Lippert–Mataga equation: a) E. Z. Lippert, *Electrochemistry* **1957**, *61*, 962–975; b) N. Mataga, Y. Kaifu, M. Koizumi, *Bull. Chem. Soc. Jpn.* **1956**, *29*, 465–470.

[14] The PL decay study showed that the contribution of the long-lived (τ_2) component increased (Table S5).

[15] Y. Dong, B. Xu, J. Zhang, X. Tan, L. Wang, J. Chen, H. Lv, S. Wen, B. Li, L. Ye, B. Zou, W. Tian, *Angew. Chem. Int. Ed.* **2012**, *51*, 10782–10785; *Angew. Chem.* **2012**, *124*, 10940–10943.

[16] a) Y. Tobe, S. Saiki, N. Utsumi, T. Kusumoto, H. Ishii, K. Kakiuchi, K. Kobiro, K. Naemura, *J. Am. Chem. Soc.* **1996**, *118*, 9488–9497; b) E. Trzop, I. Turowska-Tyrk, *Acta Crystallogr. Sect. B* **2008**, *64*, 375–382.

[17] To the best of our knowledge, the record for the largest deformation angle α is 24.3–25.6° with angle β of 23.9–26.8° for a [1.1]paracyclophane derivative is found in: H. Kawai, T. Suzuki, M. Ohkita, T. Tsuji, *Chem. Eur. J.* **2000**, *6*, 4177–4187.

[18] XRF analysis was carried out for **3**·CH_2Cl_2 and **3**·$CHCl_3$ by the detection of Cl, as shown in Figures S41 and 42, respectively, in the Supporting Information.

Received: January 7, 2015
Revised: February 6, 2015
Published online: February 27, 2015

